Atmospheric Stress Corrosion Cracking of a Superplastic 7475 Aluminum Alloy

T.C. TSAI and T.H. CHUANG

The influence of different heat treatments upon the atmospheric stress corrosion cracking (SCC) of fine-grained 7475 Al-alloy plates has been investigated. The small size of the matrix precipitates and grain-boundary precipitates (GBPs) was found to be the main cause of atmospheric SCC susceptibility. Increasing the size of the matrix precipitates and GBPs by increasing the degree of aging could improve the atmospheric SCC resistance. The size of the matrix precipitates was the major factor affecting the atmospheric SCC resistance when GBPs were larger than a critical size that could nucleate hydrogen bubbles. However, if the size of the GBPs was smaller than this critical size, the improvement of atmospheric SCC resistance due to grain refinement, resulting from a more homogeneous slip mode, could not be obtained because hydrogen embrittlement became serious. By measuring the electrical conductivity, the influence of matrix precipitates, but not that of GBPs, on SCC susceptibility could be obtained. Retrogression and reaging (RRA) treatment could effectively improve the atmospheric SCC resistance of T6 temper because RRA temper could produce larger sizes of both the matrix precipitates and GBPs than could T6 tempered condition.

I. INTRODUCTION

HIGH-STRENGTH aluminum alloys of the Al-Zn-Mg type (7xxx series) are widely used in airframe construction. These alloys are usually chosen because of their high strength and stiffness, which are derived from precipitation hardening. However, 7xxx series aluminum alloys are susceptible to stress corrosion cracking (SCC) failures observed in service, particularly when they are aged to the near-peak strength T6 tempered condition.[1–4] Their resistance to SCC can be increased by overaging to T73 temper but with a concomitant loss of about 10 to 15 pct in strength. Cina[5] has reported a heat treatment known as retrogression and reaging (RRA), which was claimed to give SCC resistance equivalent to that of T73 temper together with T6 strength levels.[6–9] This treatment has been applied to materials in the T6 condition and consists of reheating the material for a short time in the temperature range of 200 °C to 280 °C (retrogression treatment), followed by reaging using the same conditions as in the original T6 age. An optimum condition chosen for SCC testing was retrogression for 5 minutes at 220 °C, followed by reaging, which produced the best SCC results.[7,10]

Burleigh[4] summarized three main mechanisms for SCC in aluminum alloys. They are anodic dissolution, hydrogen-induced cracking, and passive film rupture.[2,3] He also indicated that anodic dissolution is generally favored in the 2xxx series aluminum alloys, whereas hydrogen-induced cracking is favored in the 7xxx series. The SCC susceptibility of 7xxx series aluminum alloys is well known to be strongly affected by their microstructural characteristics. Three principal microstructural features have been discussed concerning the influence of SCC. They are the precipitate free zone (PFZ), matrix precipitate structure, and grain-boundary precipitate (GBP) structure.[11–14] Generally, overaging can improve the SCC resistance of high-strength aluminum alloys by means of the more homogeneous slip mode and the reduction of slip planarity, which are due to the increase of matrix precipitate size and the associated change from GP zones to semicoherent η' and incoherent η precipitates.[14,15,16] The homogeneous slip mode can effectively reduce either stress-assisted anodic dissolution along grain boundaries[17] or hydrogen transported to the grain boundaries for inducing cracking by means of mobile dislocations.[15,17] On the other hand, the increasing size of GBPs during overaging has been proposed to explain the higher SCC resistance in the 7xxx series aluminum alloys.[8,13] The larger η precipitates in the grain boundary can act as sacrificial anodes[13] or as trapping sites for atomic hydrogen to retard intergranular SCC.[8,10,18] By trapping atomic hydrogen, the bubbles of molecular hydrogen nucleate at GBPs, thus lowering the concentration of atomic hydrogen in the grain boundary and preventing hydrogen embrittlement, which is due to atomic hydrogen-reducing grain boundary cohesion.[18,19] The influence of the PFZ on SCC susceptibility is uncertain, as previously reported by some authors.[12,20] Increasing the width of the PFZ may lead to improvement or reduction or may have no effect on SCC susceptibility.

Grain refinement can be made by thermomechanical treatment for high-strength aluminum alloys and frequently results in beneficial effects for mechanical properties, such as yield strength, ductility, fracture toughness, and fatigue life.[21,22] Another significant effect produced by grain refinement is that on the character of deformation at high temperatures, which is superplastic.[22,23] Fine-grain microstructure in high-strength aluminum alloys, such as 7475 aluminum alloy, can be developed and applied in air frame constructions by means of superplasticity.[24] Generally, fine-grain structure presents smaller size of GBPs[25] and superplastic forming will cause decay of the mechanical properties in the alloy because of the formation of cavity and grain growth.[26,27] It means that the unsuitable tempers

T.C. TSAI, Doctoral Candidate, and T.H. CHUANG, Professor, are with the Institute of Materials Science and Engineering, National Taiwan University, Taipei, Taiwan, 106, Republic of China.

Manuscript submitted April 24, 1995.

Table I. Chemical Compositions (Weight Percent) of the 7475 and 7075 Aluminum Alloys

Alloy	Zn	Mg	Cu	Cr	Fe	Si	Mn	Ti	Al
7475	5.80	2.24	1.53	0.19	0.08	0.02	< 0.06	< 0.02	bal
7075	5.76	2.46	1.70	0.20	0.12	0.09	< 0.30	< 0.20	bal

Table II. Heat Treatment Procedures for Alloys Investigated

Temper	Condition	Aging Treatment
T4*	underaged	as–naturally aged to stable
T6**	near peak aged	24 h/120 °C
RRA**	peak aged	T6 aged + 5 min/220 °C + T6 aged
T73**	overaged	6 h/107 °C + 24 h/163 °C
FC†	overaged	as–furnace cooled

*As received.
**Solution treated at 515 °C for 1 h + water quenched.
†Solution treated at 515 °C for 1 h.

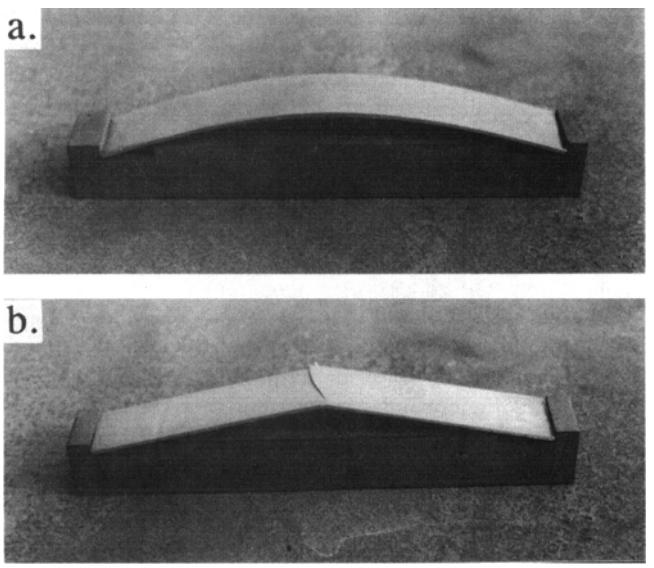

Fig. 1—Two-point loaded bent-beam specimens used in atmospheric SCC tests: (*a*) appearance of SCC specimen before failure and (*b*) appearance of SCC specimen after failure.

or microstructural conditions will cause serious SCC damage in the superplastically formed workpieces.

Previous investigations have paid much attention to the SCC resistance of aluminum alloys. However, reports on atmospheric SCC testing have been very rare, particularly on aluminum alloys.[28,29] The purpose of this investigation was to evaluate the influence of the microstructural features on atmospheric SCC susceptibility. Transmission electron microscopy (TEM) quantitative data were characterized by the width of the PFZ and the size of the matrix and grains-boundary precipitates to identify the relationship between the microstructure and the SCC susceptibility.

The chemical composition of the 7075 aluminum alloy is similar to that of the 7475 alloy.[7] A commercial, 2-mm thickness 7075 Al-alloy plate possessed a grain size of about 50 μm and its chemical composition is shown in Table I. The atmospheric SCC resistance of this 7075 alloy was used to compare with that of the fine-grained 7475 alloy in the T6 tempered condition. It is helpful for clearly analyzing the influence of microstructure upon the atmospheric SCC susceptibility and the electrical conductivity in this study.

II. EXPERIMENTAL PROCEDURE

The material used in this study was a commercial superplastic 7475 aluminum alloy in T4 tempered condition. This material was supplied as a 2-mm-thick plate. The nominal chemical composition is listed in Table I, and all the heat-treatment procedures are described in Table II.

The longitudinal (L) direction of all the tempered materials was characterized by tensile strength, electrical conductivity, and atmospheric SCC susceptibility. Rectangular tensile specimens with a gage length of 25 mm and a width of 6.25 mm were used. Tensile tests were performed at a strain rate of 10^{-3} s^{-1} in air. The electrical conductivity was measured by using the conventional four-probe method. Using a KEITHLEY Model 220 programmable current source and Model 182 sensitive digital voltmeter, the values of the electrical conductivity in units of $(\Omega \cdot cm)^{-1}$ could be obtained.

Atmospheric SCC tests were performed on two-point loaded bent-beam specimens according to ASTM Standard G-39-79. One typical sample is shown in Figure 1(a). Three specimens for each heat-treatment condition were milled to 27-mm width, 2-mm thickness, and the exact length required to produce applied stresses of 90 and 70 pct of their 0.2 pct yield strength in the extreme outer fibers of the center section of each specimen when fitted into two-point-loaded 18-cm-long jigs. The following formula was used for these calculations.[29]

$$\text{Specimen length} = \frac{0.0244tE}{\sigma} \sin^{-1} \frac{L\sigma}{1.4tE}$$

where

t = specimen thickness = 2 mm;
E = Young's modulus;
σ = stress desired in outer fiber; and
L = jig length = 18 cm.

The angle was measured in degrees. The correction factor of 1.4 adjusted the calculated stresses to within 3 pct of the levels measured experimentally. Before atmospheric SCC tests, the bent-beam specimen surfaces were polished manually with 100-grit abrasive paper to remove heat-treating traces and any visible surface defects. This treatment was followed by fine polishing with abrasive paper until 600-grit, then degreasing with acetone, washing in distilled water, and drying with hot air. These specimens were exposed on test racks and tilted 30 deg horizontally, at an outdoors site at National Taiwan University (Taipei, Taiwan). This is a moderately corrosive city environment. The weather and atmospheric corrosion pollutant information are listed in Tables III and IV, respectively.[30] Inspection of the exposed specimens was performed daily for the first month and twice a week thereafter. A specimen was con-

Table III. The Referential Weather Data in Exposed Location of Atmospheric Stress-Corrosion Tests*[30]

Temperature (°C)	Relative Humidity (Pct)	Sunshine (h/day)	Rain (h/day)	Rain Fall (mm/day)	Wind Speed (m/s)
23.1	77.9	3.6	3.6	7.2	3.0

*Data indicate the average values from May 1987 to May 1990.

Table IV. The Referential Atmospheric Corrosion Pollutants' Concentration in Exposed Location of Atmospheric Stress-Corrosion Tests*[30]

$[H^+]$ (meq/L)	$[SO_4^{-2}]$ (mq/L)	$[Cl^-]$ (mq/L)	$[NO_3^-]$ (mq/L)
2.57×10^{-5}	4.59	3.12	1.55

*Data indicate the average values from May 1987 to May 1990.

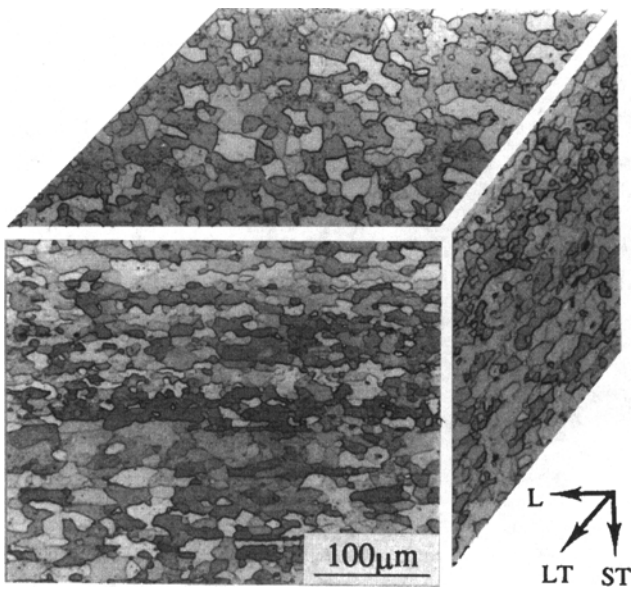

Fig. 2—Three-dimensional micrograph showing the grain structure of the as-received 7475-T4 alloy plate.

Table V. Intercept Grain Size of the 7475 Aluminum Alloy

Alloy	Longitudinal Direction (μm)	Long Transverse Direction (μm)	Short Transverse Direction (μm)
7475	12.5	12.1	9.2

Table VI. Mechanical Properties of the Tensile Tests for Various Tempers of the 7475 Aluminum Alloy

Temper	Ultimate Strength (MPa)	Yield Strength (MPa)	Elongation (Pct)
T4	569.1	461.5	20.0
T6	579.6	515.1	15.4
RRA	564.4	531.1	10.1
T73	517.3	450.2	12.3
FC	331.1	186.3	14.5

sidered to have failed if it fractured or contained a crack that was visible to the unaided eye.

Optical microscopy (OM) and TEM were utilized to observe the microstructural change. Samples for OM were

Table VII. Results of Atmospheric Stress-Corrosion and Electrical Conductivity Tests for Various Tempers

Temper	Average Time to Failure (Days) 70 pct*	90 pct*	Electrical Conductivity $\times 10^6(\Omega \cdot cm)^{-1}$	(pct IACS)
7475-T4	15	6	0.165	(28.4)
7475-T6	55	34	0.189	(32.6)
7075-T6	NF†	NF	0.182	(31.4)
7475-RRA	NF	NF	0.224	(38.6)
7475-T73	NF	NF	0.239	(41.2)
7475-FC	NF	NF	0.258	(44.5)

*Applied stress levels are given in terms of percent of yield strength.
†NF indicates no failure found until the submitted day of this article (tests began on May 2, 1994 for all tempers).

chemically etched in Keller's Reagent, and thin foils were prepared by twin-jet electropolishing in a 33 pct HNO_3 + 67 pct methanol solution cooled to −25 °C, using a potential of ~12 V. The TEM quantitative data for the width of the PFZ, the GBP population and size, and the size of the matrix precipitates (semicoherent η' and incoherent η) were characterized by a JEOL* 100CXII TEM operating at 100

*JEOL is a trademark of Japan Electron Optics Ltd., Tokyo.

kV. The PFZ width, the GBP size, and the number of GBPs per unit area were determined by using the methods described previously.[31] Slip behavior was investigated using prestrained tensile specimens which were slowly strained to a plastic strain of 4 pct. Thin foils were made from these specimens and observed in the TEM. Under the same two-beam conditions, the foils were tilted until the slip bands were visible and normal to an operating $\langle \bar{1}\,\bar{1}1 \rangle$ **g** vector.[14,31] Fractography of all failed atmospheric SCC specimens was conducted with a PHILIPS* SEM515 + EDAX scanning

*PHILIPS is a trademark of Philips Electronic Instruments Corp., Mahwah, NJ.

electron microscope (SEM) operating at 20 kV.

III. RESULTS

A three-dimensional optical micrograph of the as-received 7475 aluminum alloy plate reveals a fine-grained microstructure, as shown in Figure 2. Any obvious microstructural difference could not be found for the other heat-treatment conditions. The mean intercept grain dimensions for this investigated alloy are listed in Table V. It shows a less anisotropy of about 30 pct in grain shape.

The mechanical properties of the tensile test are shown in Table VI. The yield strength evidently was increased from T4, through T6 to RRA tempered, and decreased from RRA, through T73 to FC tempered condition. However, the elongation revealed the opposite relationship of the yield strength. The higher values of elongation for all various tempers of 7475 alloy, as demonstrated in Table VI, are a result of grain refinement.[21] The aging treatment conditions for all the heat treatments are indicated in Table II. They show an aging sequence from T4 to FC tempered condition. The RRA temper produced the highest yield strength and the smallest elongation and also showed a peak-aged condition.

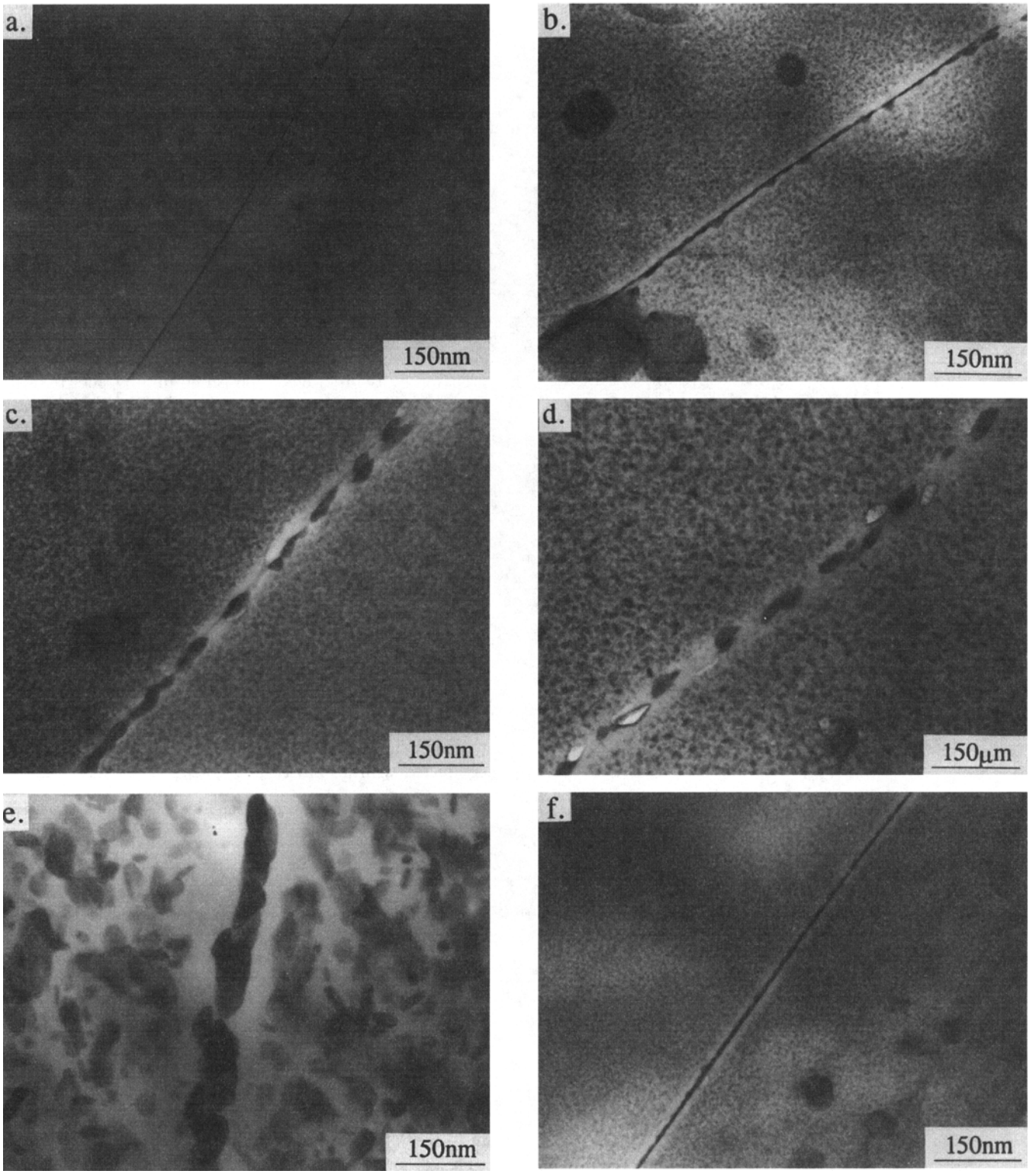

Fig. 3—TEM micrographs showing the precipitate-free zone width of the various tempers: (*a*) 7475-T4, (*b*) 7475-T6, (*c*) 7475-RRA, (*d*) 7475-T73, (*e*) 7475-FC, and (*f*) 7075-T6.

The results of atmospheric SCC tests are given in Table VII. The times to failure were obtained from the average of three testing specimens. Only 7475-T4 and 7475-T6 tempered specimens could be found to fail within 55 days. One typical appearance of some cracked specimens for atmospheric SCC tests is shown in Figure 1(b). Unfailed specimens of atmospheric SCC tests continue to be exposed for obtaining the times to failure. The values of electrical conductivity for the various heat treatments are also indicated in Table VII. The electrical conductivity of the 7475 alloy increased with the increasing degree of aging. The FC and T4 tempered conditions possessed the largest and the small-

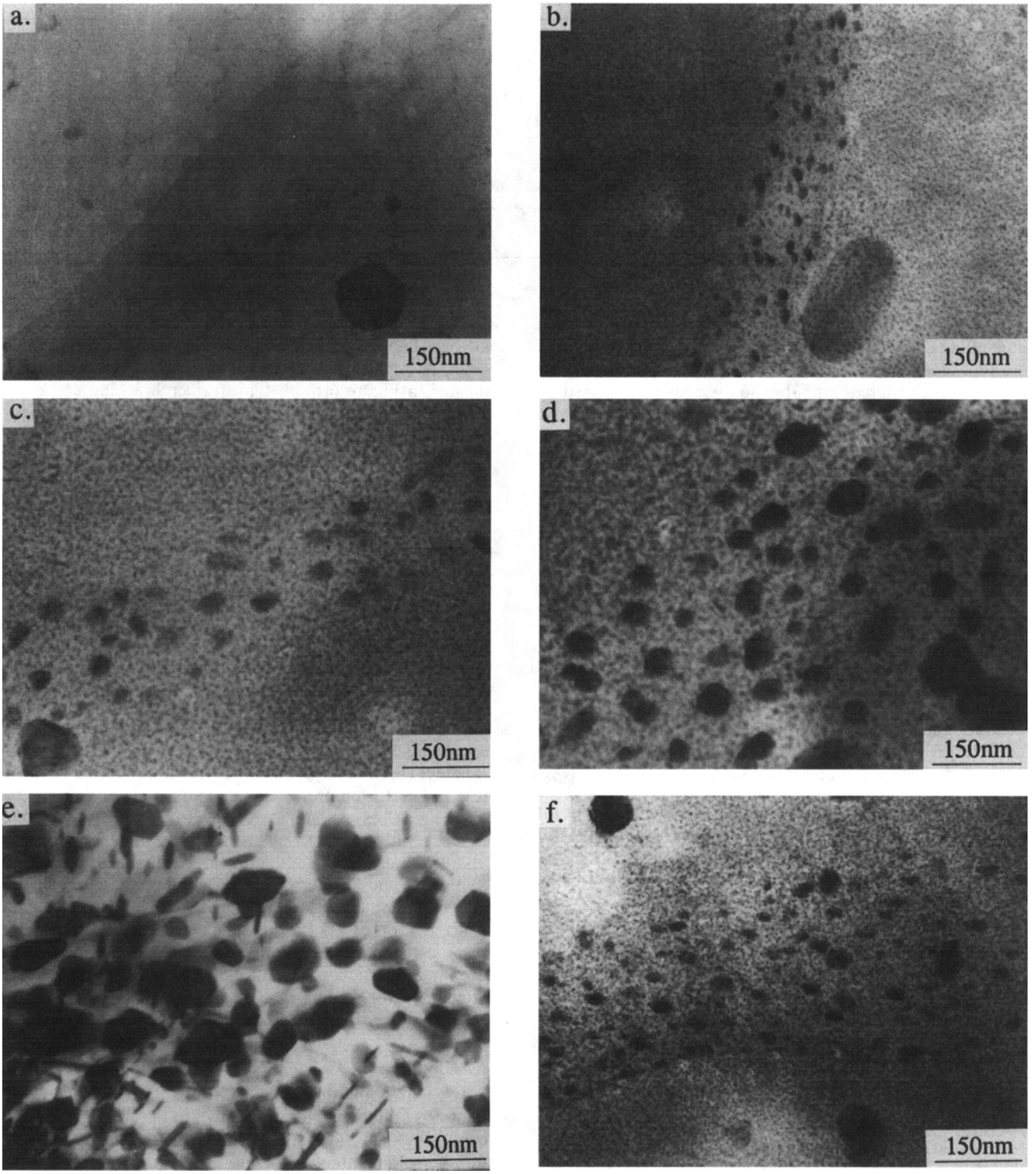

Fig. 4—TEM micrographs showing the GBPs of the various tempers: (*a*) 7475-T4, (*b*) 7475-T6, (*c*) 7475-RRA, (*d*) 7475-T73, (*e*) 7475-FC, and (*f*) 7075-T6.

est values, respectively. From ASTM Standard B193-87, the units of $(\Omega \cdot \text{cm})^{-1}$ for electrical conductivity can convert to the units of pct IACS (percentage of International Annealed Copper Standards) at 20 °C. Measurement of electrical conductivity was performed at 20 ± 1 °C in this investigation. Therefore, the approximate values of electrical conductivity with units of pct IACS could also be obtained and are listed in Table VII.

The PFZ widths for various heat-treatment conditions are shown in Figure 3. The PFZ widths of the 7475 alloy were found to vary and increase with the increasing degree of aging. Typical grain-boundary η precipitates for various

Table VIII. Characteristics of Microstructures for Various Heat Treatment Conditions

Temper	PFZ Width (nm)	Grain Boundary Precipitates				Matrix Precipitates	
		$\bar{d}_P$* (nm)	$\bar{\lambda}_P$ (nm)	$\bar{N}_A$ (PPTs/μm^2)	f_P** (Pct)	Type	Size* (nm)
7475-T4	7	3.9 ± 0.9	13.4	1400	2	GP zones + η' + η	2.6 ± 0.5
7475-T6	28	18.8 ± 4.5	25.0	400	13	GP zones + η' + η	5.4 ± 1.3
7075-T6	29	24.5 ± 5.6	27.1	340	18	GP zones + η' + η	4.9 ± 1.0
7475-RR	37	33.1 ± 6.8	34.1	215	21	η' + η	8.9 ± 1.6
7475-T73	45	45.6 ± 12.2	44.7	125	23	η' + η	11.6 ± 2.8
7475-FC	140	59.6 ± 17.4	48.8	105	33	η	31.4 ± 10.3

*Data indicate mean ± one standard deviation.
**Calculated using the mean values for $\bar{d}_P$ and $\bar{N}_A$.

tempers are indicated in Figure 4. Only high-angle GBP sizes and distributions were characterized by calculating precipitate diameters, $\bar{d}_p$, intraplanar spacings, $\bar{\lambda}_p$, numbers per unit area, $\bar{N}_A$, and areal fractions, f_p.[14] More than 100 GBPs in five different grain-boundary areas were measured for each heat-treatment condition to obtain the data of $\bar{d}_p$, $\bar{\lambda}_p$, and $\bar{N}_A$. Areal fractions, f_p, were estimated by the average values for $\bar{d}_p$ and $\bar{N}_A$.[31] The sizes and types of matrix precipitates were directly derived from bright-field micrographs. At least 100 precipitates were measured to get the matrix precipitate sizes for the various tempered conditions. The results of microstructural characteristics for different heat treatments are summarized in Table VIII. The value of every microstructural parameter, besides $\bar{N}_A$, increased with the increasing degree of aging for the 7475 aluminum alloy.

Figure 5 shows the slip behaviors for various heat treatments after 4 pct plastic strain. These micrographs were obtained under the same diffraction condition and magnification. The results of statistical analysis of slip-band spacings are given in Table IX. The following points should be noted from Figure 5 and Table IX.

(a) The T4 temper showed the largest slip-band spacing for the 7475 aluminum alloy, and the spacing decreased from the T4 to the T73 tempered condition. However, the distinction of slip-band spacings was very small for all tempers, and the slip-band spacings were less than 0.1 μm because of the fine-grained structure. On the other hand, the slip-band lengths also showed the same tendency as did the slip-band spacings.
(b) For the 7475 aluminum alloy, the longest and the closest dislocation distributions were revealed in the T4 tempered condition. The length and density of dislocation lines decreased with the increasing degree of aging. This phenomenon is presumably due to the increase of the volume fraction of the η precipitates and dislocation cross-slip and looping at incoherent η precipitates.[14]
(c) The 7075-T6 tempered condition had wider slip-band spacing and longer dislocation distributions than did the 7475-T6 alloy because the grain size of the 7075 alloy was larger than that of the 7475 alloy.[32]
(d) The types of matrix slip could be obtained and shown in Figure 5. The T4, T6, and RRA tempered conditions were clearly demonstrated to be planar slip types, and the T73 tempered condition was shown to be a wavy slip type. The FC tempered condition can be reasonably inferred to be a wavy slip type.

Some nonuniform distributions of corrosion pittings and crevices on the surfaces of atmospheric SCC specimens are shown in Figure 6(a). This phenomenon could be found for all heat-treatment conditions. These pittings and crevices could be found to occur almost at grain boundaries, as indicated in Figure 6(b). A typical microbraching crack and an intergranular fracture surface on the failed atmospheric SCC specimens are shown in Figures 6(c) and (d), respectively.[20] These two phenomena only could be found in the 7475 alloy with the T4 and T6 tempers until now. The initiation of atmospheric SCC is indicated from this experimental evidence to occur at corrosion crevices of the grain boundaries.[11,33] This result implies that the prolongation of the incubative period, which incurs the initiation of atmospheric SCC, is the major factor leading to improvement of the atmospheric SCC resistant of RRA, T73, and FC tempers of the 7475 alloy.

Some typical corrosion products near a corrosion crevice are indicated in Figure 7(a). The differences of element constitutions between the matrix of the 7475 alloy and the corrosion products on the surface of the atmospheric SCC specimens were revealed by energy-dispersive X-ray spectrometer (EDS) analysis and are shown in Figures 7(b) and (c). The corrosion products are demonstrated in Figure 7(c) to be the Al-oxysulfate, as indicated in a previous work.[34] Sereda[35] inferred that NaCl and SO_2 are the major contents of the atmospheric population affecting metal corrosion. Sydberger and Vannerberg[36] also found that the corrosion rate of aluminum alloys was increased by increasing the concentration of SO_2 in the atmosphere. SO_2 is considered to be a more important environment factor from the preceding discussion to produce the corrosion pittings and crevices of 7475 aluminum alloy.

IV. DISCUSSION

High-strength aluminum alloys stressed in the short transverse direction are well known to have more SCC susceptibility than those stressed in the longitudinal and long transverse directions.[1] Therefore, it is important to pay attention to the poor atmospheric SCC properties in the L direction of undeformed superplastic 7475 aluminum alloy with the T4 and T6 tempered conditions in this study.

According to some correlation studies,[7,37] the electrical conductivity could be used as a valid measure of SCC resistance. The SCC resistance has been found to increase with increasing values of electrical conductivity. The values of electrical conductivity for all various tempers of 7475 alloy, as shown in Table VII, seem to satisfy a proportional relationship of electrical conductivity and atmospheric SCC

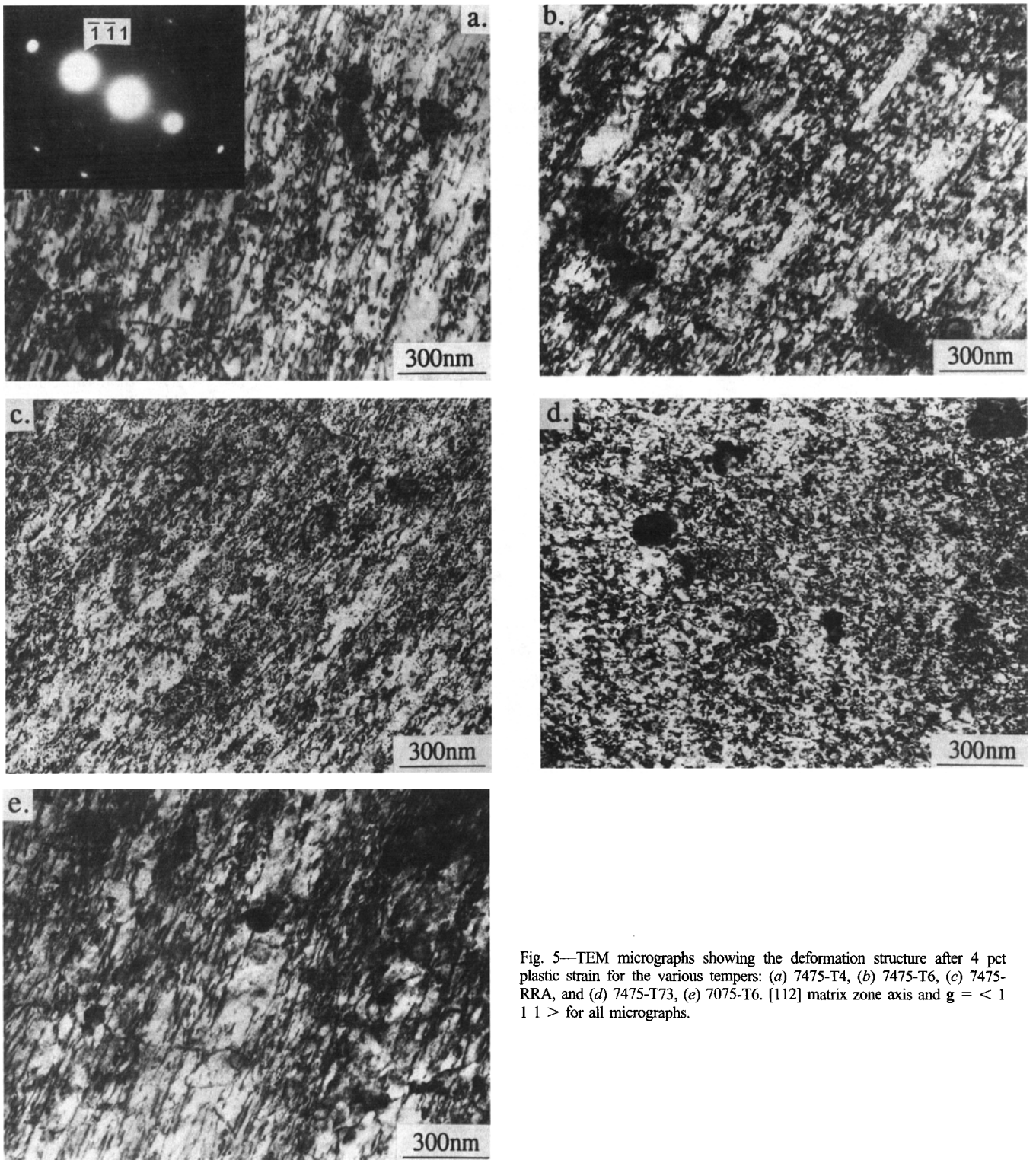

Fig. 5—TEM micrographs showing the deformation structure after 4 pct plastic strain for the various tempers: (*a*) 7475-T4, (*b*) 7475-T6, (*c*) 7475-RRA, and (*d*) 7475-T73, (*e*) 7075-T6. [112] matrix zone axis and $\mathbf{g} = < 1\ 1\ 1 >$ for all micrographs.

resistance. In fact, it is more appropriate to consider that electrical conductivity increases with increasing degree of aging[7,37] because the main factor leading to an increase in the value of electrical conductivity, obviously derived from the TEM observations and Table VIII, is that the matrix precipitates change from GP zones to semicoherent η' and incoherent η precipitates and increase the size and volume fraction of η' and η precipitates. The SCC resistance has also been inferred by some authors to improve with an increase in the size of matrix precipitates.[11,14] Therefore, the electrical conductivity could be concluded from the preceding discussion to respond to the influence of matrix precipitates on atmospheric SCC. However, the proportional relationship of the electrical conductivity and atmospheric SCC resistance cannot be obtained from a comparison with the 7475-T6 and 7075-T6 tempered alloys. The atmospheric SCC resistance of 7075-T6 tempered alloy is better than that of 7475-T6 tempered alloy, but the electrical con-

Table IX. Slip Behavior for Various Tempers*

Temper	Spacing (nm)	Type
7475-T4	84 ± 16	planar
7475-T6	68 ± 12	planar
7075-T6	105 ± 22	planar
7475-RRA	53 ± 7	planar
7475-T73	<40	wavy
7475-FC	—	wavy

*Data indicate mean ± one standard deviation.

ductivity of 7075-T6 alloy is slightly less than that of 7475-T6 alloy. This implies that there is another factor which affected the atmospheric SCC resistance besides the matrix precipitates.

Grain refinement often results in the improvement of mechanical properties, which includes SCC resistance.[21] Gruhl[32] stated that the reduction of slip-band formation is a result of grain refinement, which decreases intercrystalline fracture and SCC susceptibility. 7075-T6 tempered alloy is shown from a comparison of Figures 5(b) and (e) to possess wider slip-band spacings and longer dislocation distributions than the 7475-T6 tempered alloy because the grain size of 7075-T6 alloy is larger than that of 7475-T6 alloy.[32] Therefore, the atmospheric SCC susceptibility of 7075-T6 tempered alloy could be inferred from the foregoing discussions to be larger than that of 7475-T6 tempered alloy. However, the atmospheric SCC resistance of 7075-T6 alloy is shown in Table VII really to be better than that of 7475-T6 alloy. It means that the decrease of the atmospheric SCC susceptibility that is attributed to the reduction of the slip-band spacing by means of grain refinement cannot be obtained in 7475 alloy with a very fine grain size of about 10 μm. These results also imply that there is another factor affecting the atmospheric SCC resistance other than the slip behavior.

The tendency of decreasing SCC susceptibility with increasing precipitate sizes of matrix and grain boundary, for 7475 alloy, is shown clearly in Table VIII. The sizes of both the matrix precipitates and GBPs are revealed to control SCC susceptibility. Fine-distributed matrix precipitates can be sheared by moving dislocation, which results in long dislocation lines and planar arrays. The longer dislocation lines can provide hydrogen transport over a longer distance and a more localized hydrogen distribution at the ends of slip lines. Under the influence of the applied tension stress, hydrogen is transported and stored up at the intersection of dislocation and grain boundary by mobile dislocations, which cause severe hydrogen embrittlement and intergranular SCC. By increasing the degree of aging in 7475 alloy, the size of matrix precipitates increased, then the length and density of dislocation lines (Figure 5 and Table IX) decreased, and the slip behavior became more homogeneous. This result could lead to the reduction of stress field on the grain boundaries[9] and the inhibition of atomic hydrogen transportation,[14] it would be more difficult to occur at the initiation of cracking and to reach a critical hydrogen concentration required to embrittle the grain boundary.[18]

The larger η precipitates in the grain boundary can act as trapping sites for atomic hydrogen to nucleate hydrogen bubbles. This result could reduce the hydrogen concentration to below a critical value to retard hydrogen embrittlement and improve SCC resistance.[8,10,18] Christodoulou and Flower[18] found a critical size of approximately 20 nm for GBPs, which is required for nucleation of hydrogen bubbles. This implies that the size of GBPs must be larger than this critical size to nucleate hydrogen bubbles and then effectively reduce hydrogen embrittlement and SCC susceptibility. The average diameters of GBPs in the T4 and T6 tempered conditions of 7475 alloy are indicated in Table VIII to be smaller than 20 nm. These smaller sizes of GBPs in the T4 and T6 tempers of 7475 alloy are suggested to be the most possible factors causing serious atmospheric SCC susceptibility. Ardo and Townsend[11] reported that the size of matrix precipitates is more effective in controlling SCC susceptibility than GBPs. However, it is interesting to find that the size of GBPs is larger than 25 nm for all heat-treatment conditions. The average GBPs size of 7075-T6 tempered alloy is also about 25 nm, as shown in Table VIII. It means that the size of 25 nm is larger than the critical size for nucleating hydrogen bubbles, and the 7075-T6 alloy has more fraction of GBPs that are larger than this critical size than the 7475-T6 alloy. This is the main reason the atmospheric SCC resistance of the 7075-T6 alloy is better than that of the 7475-T6 alloy.

The following conclusions about the influence of microstructural features on atmospheric SCC can be observed from the preceding discussions. The size and type of matrix precipitates are the major factors influencing atmospheric SCC resistance when GBPs are larger than a critical size that can nucleate hydrogen bubbles. Increasing the size of matrix precipitates leads to a more homogeneous slip type, which can reduce the stress field and atomic hydrogen to pile up at the intersection of dislocation and grain boundary. On the other hand, if GBPs are smaller than this critical size, the atomic hydrogen concentration cannot be effectively reduced below a critical value to retard hydrogen embrittlement, and the SCC susceptibility would become serious. Based on the similar width of PFZ between the 7475-T6 tempered and 7075-T6 tempered alloys (Table VIII) it appears that the PFZ width has no effect on atmospheric SCC susceptibility. Finally, it can be inferred that the electrical conductivity cannot respond to the influence of GBPs on atmospheric SCC based upon the preceding discussion.

Grain refinement by thermomechanical treatment generally presents a more homogeneous slip mode and a smaller size of GBPs for the 7xxx series aluminum alloys.[25,32] The more homogeneous slip mode is the major factor that can improve atmospheric SCC by means of grain refinement. However, for a very fine grain size of about 10 μm, as investigated in this study, it is important to see that this very fine grain size will lead to the existence of fine GBPs that are smaller than a critical size of about 20 nm and cause serious atmospheric SCC susceptibility. When a small grain-size structure possesses a large number of fine GBPs that are below a critical size of hydrogen bubbles' nucleation, it means that this kind of grain structure has more grain boundaries with weak cohesive strength, which will cause a greater probability for crack initiation and a shorter distance for crack propagation. These factors would result in more rapid hydrogen embrittlement and intergranular SCC, and the benefit of improving SCC by means of grain refinement could not be obtained.

The RRA tempered condition could effectively improve

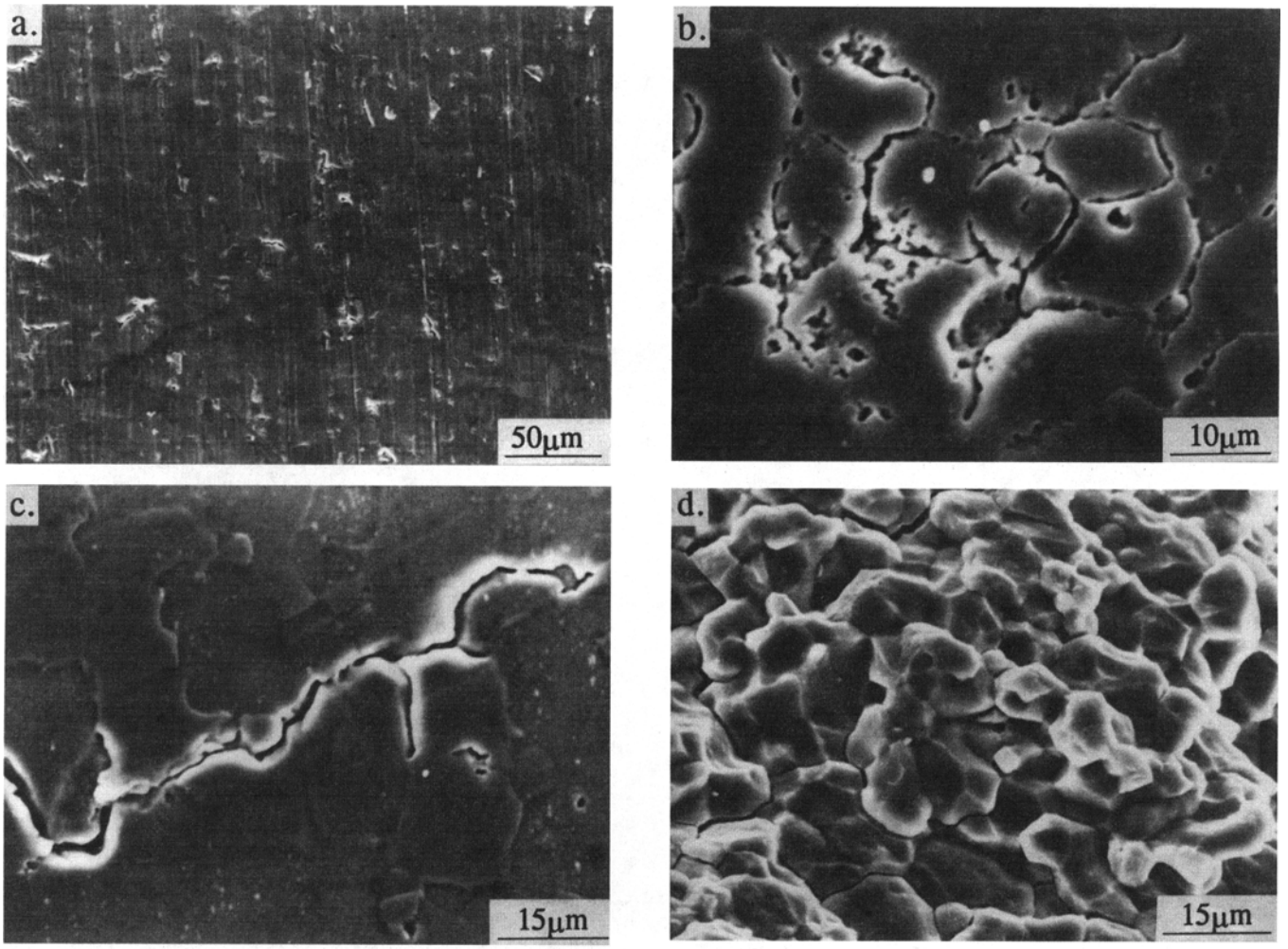

Fig. 6—Scanning electron micrographs of typical failed atmospheric SCC test specimens. (*a*) nonuniform distribution of corrosion pittings and crevices on the surfaces of atmospheric SCC specimens; (*b*) pittings and crevices found at grain boundaries; (*c*) microbraching crack on failed atmospheric SCC specimens; (*d*) intergranular fractuer surface on failed atmospheric SCC specimens.

the atmospheric SCC resistance of 7475 alloy in the T6 temper and did not sacrifice mechanical strength. It is suggested that the RRA tempered condition can provide a larger size of GBPs to reduce SCC susceptibility[8,10] and a greater volume fraction of coherent matrix precipitates to retard the loss of strength[6,10] than can the T6 tempered condition. The average GBP diameter in the RRA treatment could be found to be 33 nm. It is apparent that this size can effectively trap the atomic hydrogen in bubbles nucleated at GBPs, inhibiting the hydrogen embrittlement. Talianker and Cina[9] showed that the disappearance of dislocation is the main factor in improving SCC resistance by RRA treatment. Jacobs and Nguyen[14] also found that 7075 showed high SCC resistance when the matrix precipitate sizes were above 8.5 and 9.3 nm, respectively. Certainly, RRA temper causes a decrease in the length and density of dislocation lines, producing an average matrix precipitate size of 8.9 nm in this study. Therefore, from the large difference of SCC susceptibility between T6 and RRA, it can be concluded that RRA temper could produce larger sizes of both the matrix precipitates and GBPs than could the T6 tempered condition.

V. CONCLUSIONS

From the preceding results and discussion, the following conclusions were observed.

1. As-received superplastic 7475 Al-alloy (T4 tempered) and T6 heat-treated materials in longitudinal direction were found to suffer atmospheric SCC. Under applied stresses of 70 pct of their 0.2 pct yield strength, both specimens failed within 55 days in the city atmospheric environment.
2. A relationship between the precipitate sizes of the matrix and grain boundary and atmospheric SCC susceptibility has been found. Matrix precipitates play a major role for atmospheric SCC resistance when GBPs are larger than a critical size that can nucleate hydrogen bubbles. However, if GBPs are smaller than this critical size, serious atmospheric SCC susceptibility occurs and the influence of matrix precipitates on atmospheric SCC resistance will not be obvious.
3. The electrical conductivity used as a valid measure of SCC resistance can respond to the influence of matrix

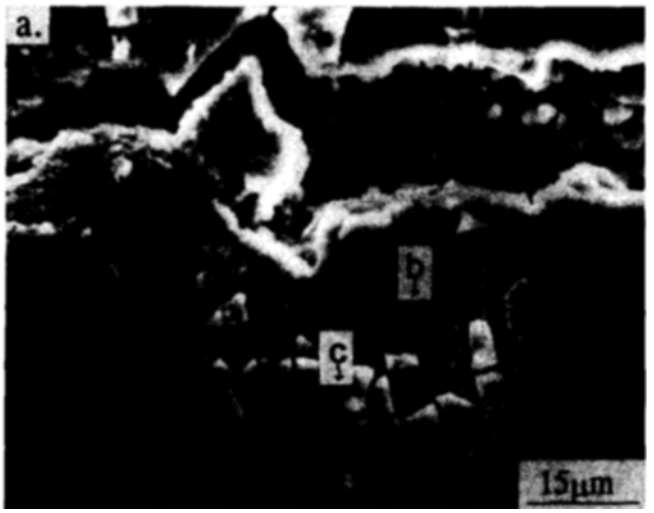

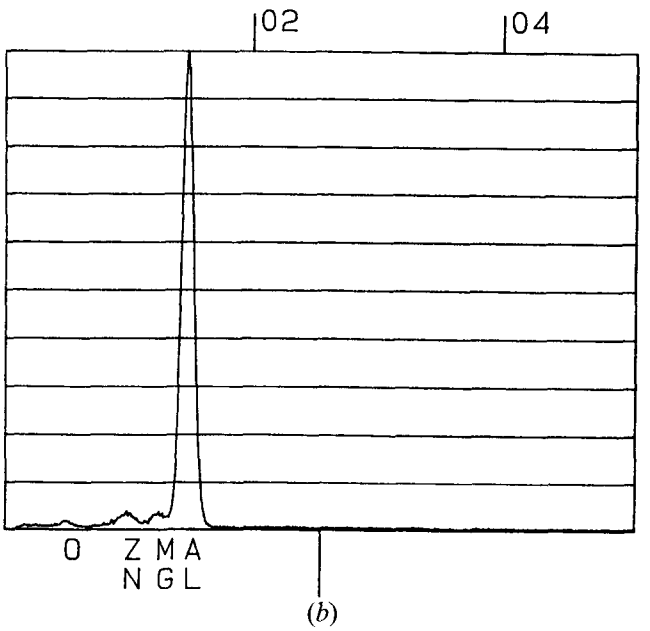

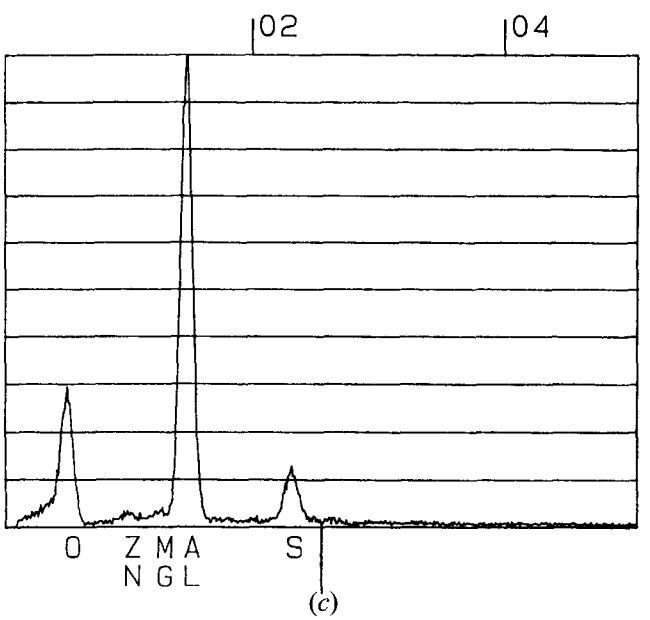

Fig. 7—(*a*) Some typical corrosion products near a corrosion crevice; (*b*) EDS of the matrix of 7475 Al alloy; and (*c*) EDS of the corrosion products.

precipitates on SCC susceptibility but cannot respond to the effect of GBPs concerning SCC susceptibility.

4. After RRA tempered treatment, the atmospheric SCC resistance of the superplastic 7475 aluminum alloy is comparable to that by T73 condition while not sacrificing the strength by the T6 temper. This is because RRA temper can produce a larger size of both matrix precipitates and GBPs than can the T6 temper.
5. A superplastically formed workpiece of superplastic 7475 aluminum alloy indicated that it is necessary to pay attention to the property of SCC susceptibility. This workpiece should use a suitable post–heat treatment, such as RRA tempered treatment, to retard SCC susceptibility.

REFERENCES

1. M.O. Speidel: *Metall. Trans. A*, 1975, vol. 6A, pp. 631-51.
2. V.A. Marichev: *Werkst. Korr.*, 1983, vol. 34, pp. 300-09.
3. W. Gruhl: *Z. Metallk.*, 1984, vol. 75, pp. 819-26.
4. T.D. Burleigh: *Corrosion*, 1991, vol. 47, pp. 89-98.
5. B.M. Cina: U.S. Patent 3856584, Dec. 24, 1974.
6. N.C. Danh, K. Rajan, and W. Wallace: *Metall. Trans. A*, 1983, vol. 14A, pp. 1843-50.
7. M.U. Islam and W. Wallace: *Met. Technol.*, 1983, vol. 10, pp. 386-92.
8. J.K. Park and A.J. Ardell: *Metall. Trans. A*, 1984, vol. 15A, pp. 1531-43.
9. M. Talianker and B. Cina: *Metall. Trans. A*, 1989, vol. 20A, pp. 2087-92.
10. K. Rajan, W. Wallace, and J.C. Beddoes: *J. Mater. Sci.*, 1982, vol. 17, pp. 2817-24.
11. A.J. De Ardo, Jr. and R.D. Townsend: *Metall. Trans.*, 1970, vol. 1, pp. 2573-81.
12. P.N. Adler, R. Deiasi, and G. Geschwind: *Metall. Trans.*, 1972, vol. 3, pp. 3191-3200.
13. P.K. Poulose, J.E. Morral, and A.J. Mcevily: *Metall. Trans.*, 1974, vol. 5, pp. 1393-1400.
14. D. Nguyen, A.W. Thompson, and I.M. Bernstein: *Acta Metall.*, 1987, vol. 35, pp. 2417-25.
15. J. Albrecht, I.M. Bernstein, and A.W. Thompson: *Metall. Trans. A*, 1982, vol. 13A, pp. 811-20.
16. J. Albrecht, A.W. Thompson, and I.M. Bernstein: *Metall. Trans. A*, 1979, vol. 10A, pp. 1759-66.
17. J.J. Thompson, E.S. Tankins, and V.S. Agarwala: *Mater. Perf.*, 1987, June, pp. 45-52.
18. L. Christodoulou and H.M. Flower: *Acta Metall.*, 1980, vol. 28, pp. 481-87.
19. G.M. Scamans, R. Alani, and P.R. Swann: *Corros. Sci.*, 1976, vol. 16, pp. 443-59.
20. M.O. Speidel: in *The Theory of Stress Corrosion Cracking in Alloys*, J.C. Scully, ed., NATO, Brussels, 1971, pp. 345-54.
21. R.J.H. Wanhill and G.F.J.A. van Gestel: *Aluminium*, 1978, vol. 54, pp. 573-80.
22. J.A. Wert, N.E. Paton, C.H. Hamilton, and M.W. Mahoney: *Metall. Trans. A*, 1981, vol. 12, pp. 1267-76.
23. D.H. Shin, K.S. Kim, D.W. Kum, and S.W. Nam: *Metall. Trans. A*, 1990, vol. 21A, pp. 2729-37.
24. In *Superplasticity and Superplastic Forming*, C.H. Hamilton and N.E. Paton, eds., TMS, Warrendale, PA, 1989.
25. J.T. Staley: ASTM STP 605, ASTM, Philadelphia, PA, 1976, pp. 71-103.
26. C.C. Bampton and R. Raj: *Acta Metall.*, 1982, vol. 30, pp. 2043-53.
27. M.W. Mahoney, C.H. Hamilton, and A.K. Ghosh: *Metall. Trans. A*, 1983, vol. 14A, pp. 1593-98.
28. K.R. Hasse and R.C. Dorward: *Corrosion-Nace*, 1986, vol. 42 (11), pp. 663-69.
29. R.R. Gaugh: *Mater. Perf.*, 1987, Feb., pp. 29-34.
30. F.T. Cheng and T.H. Chuang: *Proc. Workshop on Atmospheric Corrosion in Materials*, T.H. Chuang and C.C. Chen, eds., *National Bureau of Standards*, Taipei, Taiwan, 1991, pp. 17-30.

31. G.M. Ludtka and D.E. Laughlin: *Metall. Trans. A*, 1981, vol. 12A, pp. 2083-91.
32. W. Gruhl: *Aluminium*, 1978, vol. 54, pp. 323-25.
33. S. Ohsaki and T. Takahashi: *J. Jpn Inst. Light Met.*, 1992, vol. 42, pp. 268-73.
34. A.M. Beccaria, E.D. Mor, and G. Poggi: *Werkst. Korros.*, 1983, vol. 34, pp. 236-40.
35. P.J. Sereda: ASTM STP 558, ASTM, Philadelphia, PA, 1974, pp. 7-22.
36. T. Sydberger and N.G. Vannerberg: *Corros. Sci.*, 1972, vol. 12, pp. 775-84.
37. T. Ohnishi and H. Shiota: *J. Jpn Inst. Light Met.*, 1986, vol. 36, pp. 647-56.